Comparison and analysis of two measurement systems of horizontal atmospheric extinction of solar radiation

F. J. Barbero[a, *], G. López[c], J. Ballestrín[d], J. L. Bosch[a], J. Alonso-Montesinos[a, b], M. E. Carra[d], A. Marzo[e], J. Polo[f], J. Fernández-Reche[d], F. J. Batlles[a, b], R. Enrique[d]

[a] Department of Chemistry and Physics, University of Almería, 04120, Almería, Spain
[b] CIESOL, Joint Centre of the University of Almería-CIEMAT, 04120, Almería, Spain
[c] Department of Electrical and Thermal Engineering, Design and Projects, University of Huelva, 21004, Huelva, Spain
[d] Concentrating Solar System Unit (Plataforma Solar de Almería, CIEMAT), 04200, Almería, Spain
[e] CDEA, University of Antofagasta, 02800, Antofagasta, Chile
[f] Photovoltaic Solar Energy Unity (Renewable Energy Division-CIEMAT, 28040, Madrid, Spain
* Corresponding author. E-mail address: jbarbero@ual.es

Abstract

Direct normal irradiance is the component of solar radiation exploited by concentrating solar power plants. However, solar radiation reflected by heliostats can be partially extinguished on its way to the receivers in solar power tower plants. These energy losses are accentuated with the distance travelled by the light. The growing development of solar power tower plants has highlighted the interest in determining this phenomenon. This paper presents the results of a six-month intercomparison campaign of the two most promising extinction measuring systems. The system developed at Plataforma Solar de Almería (SE Spain) is based on a direct measurement methodology by using two digital cameras. The second system indirectly estimates the extinction from forward-scatter meter (FSM) measurements. Two FSMs were used in this study. Both FSMs provided the same Meteorological Optical Range (MOR) trends, with differences into declared error margins. A selected number of days corresponding to medium to high aerosol loads have been used to assess the performance of both types of systems. Results show that, in these days, the atmospheric extinction coefficient values derived from the two-camera system were on average 2.1 times higher than those determined with the FSMs. Semi-empirical and empirical corrections for the aerosol spectral characteristics and for the content of water vapour in the atmosphere have been applied to the FSM measurements so that both systems provide similar values of horizontal attenuation.

Keywords: Solar resource assessment, Solar power tower plant, Atmospheric extinction, Forward-scatter meters, Digital cameras.

Nomenclature

α	Aerosol Ångström exponent
σ_w	Water vapour absorption extinction coefficient
σ_{CSys}	Extinction coefficient from the CIEMAT-System
σ_{FSM}	Extinction coefficient from the FSM
$\sigma_{FSM,BB}$	FSM extinction coefficient corrected to broadband
$\sigma_{FSM\text{-}c}$	Corrected FSM extinction coefficient (km^{-1})
$\sigma_{m,\lambda}$	Molecular Rayleigh extinction coefficient at λ
ρ_{w0}	Water vapour density at the surface (g cm^{-3})

Acf	Aerosol absorption correction factor
AERONET	Aerosol Robotic Network
AOD_λ	Aerosol optical depth at wavelength λ
Att_{CSys}	Attenuation at 1 km from the CIEMAT-System
Att_{FSM}	Attenuation at 1 km from FSMs
BMod	Correction parameters set from Biral M&O manual
CIEMAT	Spanish Center for Energy and Environment Research
EMod	Correction parameters set from Elias et al. model
F_λ	Correction factor to change the spectral range
FSM-UAL	Forward-scatter meter from University of Almería
FSM-UHU	Forward-scatter meter from University of Huelva
MOR	Meteorological Optical Range (km)
PSA	Plataforma Solar de Almería (CIEMAT- Center for solar power development)
SSA	Single scattering albedo
STEP	Solar Thermal Energy Plant
StF	Aerosol scattering to fog scattering ratio
VR	Visibility Range (km)
w	Precipitable water content (cm)
WMO	World Meteorological Organization

1. Introduction

With society's increasing energy consumption, fossil fuels and their use to generate energy have multiple disadvantages, whether due to depletion, economic issues, or their negative effect on the environment. In this sense, renewable energies are presented as a clear alternative, having a lower impact on the environment compared to other energy sources. The generation through some renewable energies, such as solar or wind, has an intermittent character that varies depending on the location and its weather conditions which, in turn, vary seasonally. Therefore, its performance is conditioned by its variation in time and weather conditions. Over the next few years, it is expected that there will be an increasing dependence on the energy supply from renewable resources. In this context, concentrating solar thermal technologies, such as parabolic troughs or solar tower power plants, stand out thanks to the thermal storage that allows them to produce continuously without depending on variations in the solar resource.

A solar power tower plant basically consists of a receiver on top of a tower, surrounded by a field of heliostats. The heliostats, large mirrors that track the movement of the sun, reflect solar beam radiation towards the receiver, which absorbs the radiation and converts it into process heat. Both heliostats and receivers typically operate in the 300-2500 nm spectral range of solar radiation. The process heat produced can be used for a variety of applications, including the production of electricity using turbines. It can also be stored for later use.

It is well known that the atmosphere interacts with the beam radiation, or Direct Normal Irradiance (DNI), causing its attenuation through the processes of absorption and dispersion. This interaction determines the amount of solar resource available at ground level for use in Concentrated Solar Power (CSP) plants. To measure the amount of solar resource available at a specific location in real time, radiation sensors, such as pyrheliometers, are used. Model retrievals and satellite images also help to obtain information about the solar resource available at a specific location.

In the case of large solar power tower plants, the reflected solar radiation from the outermost heliostats must travel distances longer than 1 km to the receiver. In this second propagation through the lower layer of the atmosphere, solar radiation suffers additional attenuation processes of absorption and scattering, which can cause losses of up to 40% depending on the atmospheric conditions (Ballestrin & Marzo, 2010). This additional attenuation occurs in the optical path between the heliostats and the receiver and has a spectral character, i.e., it depends on the wavelength. It is mainly due to atmospheric aerosols and water vapour, components that are more concentrated in this lower layer of the atmosphere, which further exacerbates their effect. This attenuation translates into power losses compared to what is expected. This is a crucial aspect in the design and operation of solar power tower plants. The actual amount of useful solar radiation available at the place of interest, that which reaches the receivers, may differ from those estimated from the site's solar resource databases. It is therefore crucial to quantify these losses.

The first studies on the estimation of these power losses were carried out in the 70s and 80s based exclusively on modelling techniques (Pitman & Van't-Hull, 1982). Recently, with the increase in size and power of solar tower plants, the determination of power losses due to atmospheric attenuation has become essential. Different methodologies have been developed over time for estimating power losses (Hanrieder et al., 2017); Hanrieder et al., 2019)). These include modelling techniques and direct or indirect measurement of the atmospheric extinction using different instruments (satellites, digital cameras, ceilometers, etc). For example, power losses have been modelled using radiative transfer codes and different sets of input parameters: tower height, slant range between heliostats and the receiver, precipitable water content, or aerosol type and concentration (López et al., 2017; López et al., 2018a). A methodology to estimate the extinction of radiation in the first 150 m of the lower atmosphere and its impact on the generated electricity cost has been recently published (Marzo et al, 2021).

Due to its special characteristics, transmissometers and forward-scatter meters (FSMs), which were designed to provide information on visibility conditions on airports or highways, have been considered of interest in determining the horizontal attenuation in solar plants (Hanrieder et al., 2012); López et al., 2017a). These equipment provide information about visibility through a related parameter: the Meteorological Optical Range (MOR), defined as: "*The length of path in the atmosphere required to reduce the luminous flux in a collimated beam from an incandescent lamp at a colour temperature of 2700 K to 0.05 of its original value, the luminous flux being evaluated by means of the curve of spectral luminous efficiencies for photopic vision given by the International Commission on Illumination (C.I.E.)*" (WMO, 2014).

The Kochsmieder approximation of this definition (Kochsmieder, 1924), derived from the Beer-Lambert law, allows for the atmospheric extinction coefficient at around 550 nm to be obtained from the MOR value, using:

$$\sigma_{ext}\,[\mathrm{km}^{-1}] = \ln(0.05) / \mathrm{MOR[km]} \qquad (1)$$

The physical principle on which the design of a transmissometer is based is very similar to the definition of Meteorological Optical Range. The most common transmissometers consist of an emitter, which has a luminous source that meets the above cited conditions (light sources today are white light LEDs, whose spectrum ranges from 400 to 750 nm, with colour temperature of 2700 K) and a receiver, both separated by a distance ranging from 10 to 300 m. Light is sent from emitter to receiver, and visibility is calculated from the attenuation of the transmitted light. The atmospheric extinction in the spectral range of the instrument is derived from this measurement. However, transmissometers can present several drawbacks: 1) short distances used to perform the measurement; 2) the corresponding small sensitive atmospheric volume is a considerable source of uncertainty when the measurement is extrapolated at longer distances, and 3) they need frequent maintenance and calibration.

Monochromatic transmissometers have also been utilized to determine monochromatic horizontal atmosphere attenuation, such as the long-path LPV4 transmissometer (OPTEC, 2011). A LPV4 uses as emitter a LED at 532 nm, with 10 nm bandwidth, and it can work with large distances between transmitter and receiver, up to 20 km. It records extinction by aerosols, but needs to correct its measurement to broadband extinction. Drawbacks are that it is very sensitive to vibrations, alignment and dirt. This transmissometer has been tested at the PSA, using a distance among emitter and receiver of 487 m (Hanrieder et al, 2015).

A flip-up LIDAR system could be useful to detect irregularities in aerosol concentrations at lowermost atmosphere layers, but it would have to meet the basic condition of having a full overlap between the solid angles of emission and reception of radiation at short distances, say, one hundred meters. However, estimating the aerosol extinction coefficient along a path in that layer is a difficult task. A LIDAR system records the backscatter coefficient which is not very sensitive to the type of aerosol, and therefore to determine the aerosol extinction coefficient from the backscatter value the *lidar ratio* of the specific aerosol type is needed. Finally, if these difficulties could be avoided, the result is still a monochromatic extinction coefficient, and some algorithm must be used to have a broadband extinction value.

Because of the novelty of the problem, which was highlighted a decade ago with the advent of large tower plants, there are not many techniques for measuring atmospheric attenuation. However, quality measurements are necessary not only to measure losses in real-time, but also to generate and validate models that allow their estimation from other parameters. Two of the most promising atmospheric attenuation measurement techniques are the CIEMAT-System and those based on forward-scatter meters. The CIEMAT-System was developed at the Plataforma Solar de Almería and is based on a direct measurement methodology using two digital cameras. The second system indirectly estimates the extinction from the forward scattering meter (FSM) measurements. This paper presents the results of a six-month intercomparison campaign of the two extinction measurement systems mentioned above: CIEMAT-System and the FSM based methodology. Before that, the following section provides a literature review and contextualisation of the FMS and the CIEMAT-System. This will help to better understand the basis for the functioning of each methodology, its application and to evaluate the results of the intercomparison. Subsequently, the materials and methodology will be described, followed by the results and conclusions.

2. Forward-scatter meters and CIEMAT-System

FSMs were developed for the same purpose as transmissometers, to provide a value of visibility, but being cheaper and with lower maintenance needs. A FSM consists of an emitter, usually a narrow band LED operating in the near-infrared band (i.e. 850 nm), and a receiver located at an angle of about 45º with respect to the beam of the emitter. The receiver collects the scattered light in a sensitive volume of about 400 cm^3, at a scattering angle of about 45°. This arrangement was adopted because it was experimentally demonstrated (Middleton, 1952) that in the range of angles between 35º and 55º, the scattering coefficient has a low dependence on the size of the dispersing particles. The FSM design and operation is based on two assumptions: absorption phenomena can be neglected, and the radiation detected in the range of selected scattering angles is proportional to the total scattering extinction coefficient (Biral VPF Series, 2017). Therefore, the MOR value supplied by a FSM accounts for the scattering by the atmospheric constituents. Since the MOR is a parameter related to the visual spectral range, for a FSM to fulfill the task of providing a visibility value, it must be calibrated against a transmissometer which works in the visible spectral range. The primary calibration is usually performed in reference installations in order for both technologies to match under atmospheric conditions which may cause a significant degradation of visibility, such as fog, haze or rain (Bloemik, 2006), (Tjugum et al., 2005).

In the WMO definition, Fog is "*a suspension of very small, usually microscopic water droplets in the air, reducing visibility at the Earth's surface",* while Haze is "*a suspension in the air of extremely small, dry particles invisible to the naked eye and sufficiently numerous to give the air an opalescent appearance".*

FSMs have been designed primarily to provide visibility values under mist and fog conditions, and therefore the comparison of their measurements with those by a transmissometer is mainly performed under low visibility conditions.

Considering the low cost and low maintenance of FSMs, these devices could be used to estimate the atmospheric attenuation of solar radiation between the field of heliostats and the receiver in Solar Thermal Power Plants (STP). In this respect, (Hanrieder et al., 2015) developed a methodology to estimate the horizontal attenuation losses using MOR measurements from a FSM Vaisala-FS11 (Vaisala, 2010) at near IR, and transmittance values from a LPV4 transmissometer working at 532 nm (OPTEC, 2011), and using the *libRadtran* software package for radiative transfer to calculate the water vapour absorption. Statistical values of atmospheric transmittance at 1 km at three locations were obtained with that methodology (Hanrieder et al., 2019).

In the case of the FSM Biral-SWS250 (O&M SWS Manual, 2014), their MOR measurements (or equivalent extinction coefficients) have been well correlated with the relative humidity, pressure, air temperature and direct and diffuse irradiances, into an artificial neural network (ANN) structure. But it is worth noting that the inclusion in the ANN of the radiative variables does not result in a noticeable improvement of the fitting (López et al., 2018b).

Also, MOR measurements from the same instrument have been simulated using as input variables the relative humidity and the aerosol optical depth (AOD) at different wavelengths derived from a collocated spectroradiometer. The correlation versus AODs only is very poor, but a significant improvement is reached with the incorporation of the relative humidity as an input variable (López et al., 2018b).

FSMs have been used along with systems based on digital cameras as an automated reference instrument that may also determine the Visibility Range (VR, a parameter equivalent to 4/3 of MOR) according to the WMO definition. Chen el al. (2013) recorded visibility values using a digital camera and a Vaisala FSM FD12. They found a high level of agreement between both systems for visibility (VR) values between 1.5 and 3.0 km. Wang et al. (2013) also performed an intercomparison of the horizontal visibility values using three systems: a digital camera, a FSM-FD12 and a trained human observer. Results showed that the three methods display the same trends and a reasonable agreement in non-rainfall situations for VR values below 3.0 km. The goal in the two above cited works was to develop measurement systems based on digital cameras suitable to determine the visibility. But the performance analysis of these systems was undertaken under very low visibility conditions, less than 3 km. These extreme cases are not usual in the day-to-day STEP operation.

A system has been developed at Plataforma Solar de Almería (PSA), southern Spain, to measure the horizontal atmospheric attenuation of solar radiation in STP. It uses two identical cameras, one placed near to a black and white Lambertian target and the other one far away from the target (CIEMAT-System). A complete and detailed description of all aspects and configuration of CIEMAT-System is in (Ballestrin et al., 2018a). Attenuation measurements by the CIEMAT-System have been correlated with the relative humidity and concentration of particles (Ballestrin et al., 2020). Result shows a normalized root-mean-square deviation of 5.5% and a Pearson's coefficient of 0.92. This close dependence shows that, in principle, these two variables would be enough to explain the atmospheric attenuation. Unfortunately, particle counting systems are rare to find in the scope of a STEP.

CIEMAT-System extinction values at PSA have been well estimated (correlation coefficient R = 0.88) from radiative and meteorological variables (direct normal irradiance, atmospheric pressure, relative humidity and temperature) using ANN techniques (Alonso-Montesinos et al, 2021). This shows that the standard variables conventionally measured in solar plants can serve as a first good estimate of horizontal atmospheric extinction.

A six-month measurement campaign was undertaken at PSA, where the CIEMAT-System and two identical FSMs were jointly used. This document summarizes the comparison between both systems. Also the differences between the extinction values provided by both systems are shown, together with the possible causes that could explain them and the corrections that could be done to obtain a better agreement between both systems.

3. Material and methods

The comparison test was carried out at PSA (SE Spain; 37.0970 N, 2.3647 W, altitude 500 m a.s.l.) from February 2nd to July 22nd 2018. PSA is a Singular Scientific-Technical Installation, which belongs to the Spanish System of Science and Technology, and in which different solar receiver prototypes have been evaluated in the past two decades (PSA Annual Report, 2018). The test site is located in the desert of Tabernas (Almería, Spain), between two ranges, *Sierra de los Filabres* to the north and *Sierra Alhamilla* to the southeast, which isolate it from the humid currents of the nearby Mediterranean Sea. Its climate ranges from semi-arid to Mediterranean, with scarce rainfall (less than 200 mm per year). The southeast of the Iberian Peninsula is sometimes affected by African dust episodes with large mineral dust particle loads. But visibility conditions at PSA are otherwise excellent (Carra et al., 2018); (Ballestrin et al., 2018b).

3.1 Equipment and features

3.1.1 Two-digital camera system (CIEMAT-System)

It uses two identical Hamamatsu® ORCA cameras, one located at 83 m and other at 825 m from a Lambertian target being the distance between cameras of 742 m. The target has one half painted white with Amercoat 741 with 70% weighted solar reflectance and the other half painted black using Zynolyte® with 95% weighted solar absorptance. Both cameras simultaneously record the target image, and the horizontal extinction is derived at the distance between both cameras using a contrast formulation (Ballestrin et al., 2018a); (Ballestrín et al., 2018b).

The CIEMAT-System essentially consists of the camera's optical system, CMOS detector, cabinet borosilicate windows and neutral filters. It has been checked that all the elements have a high value of transmittance throughout the whole spectral range covered by the camera (400-1000 nm). The combination of the responses of all elements (camera, windows, filters and paint), gives a CIEMAT-System spectral response centered on 550 nm. The spectral response of the CIEMAT-System, ranging from 400 to 1000 nm, includes three water vapour bands at 720 nm, 810 nm and 940 nm, with the strongest one centered at 940 nm, whose response is around 10% of its maximum value at 550 nm. Due to this system's design, it can be stated that it records the extinction between cameras by air molecules (Rayleigh scattering), aerosols (absorption and scattering) and water vapour.

The CIEMAT-System is fully automatic and is running at PSA since June 2017 working in a supervised manner, subject to strict control of operation and verification, so that data is only taken in working days. The real time attenuation value provided by this system is displayed on the control panel of the CESA-1 thermosolar plant of the PSA.

3.1.2 Forward-scatter meters

Two Biral FSMs model SWS-250 (O&M SWS Manual, 2014) have been used in this study: one belonging to the University of Almería (UAL) and another to the University of Huelva (UHU). The SWS-250 emits an infrared light beam at wavelength of 850 nm and bandwidth around 40 nm; the receiver collects the light scattered by the atmosphere in a sensitive volume of about 400 cm^3, and at a dispersion angle of 45º with ± 6º cone angle. The SWS-250 also provides information on the meteorological situation, as the type and amount of precipitation.

Both FSMs were placed on the roof of one of the PSA buildings (Figure 1), separated by a distance of several meters, well above ground level, and oriented according to the assembly standards of this type of equipment. The selected emplacement is in the same area in which the CIEMAT-System operates (Figure 1).

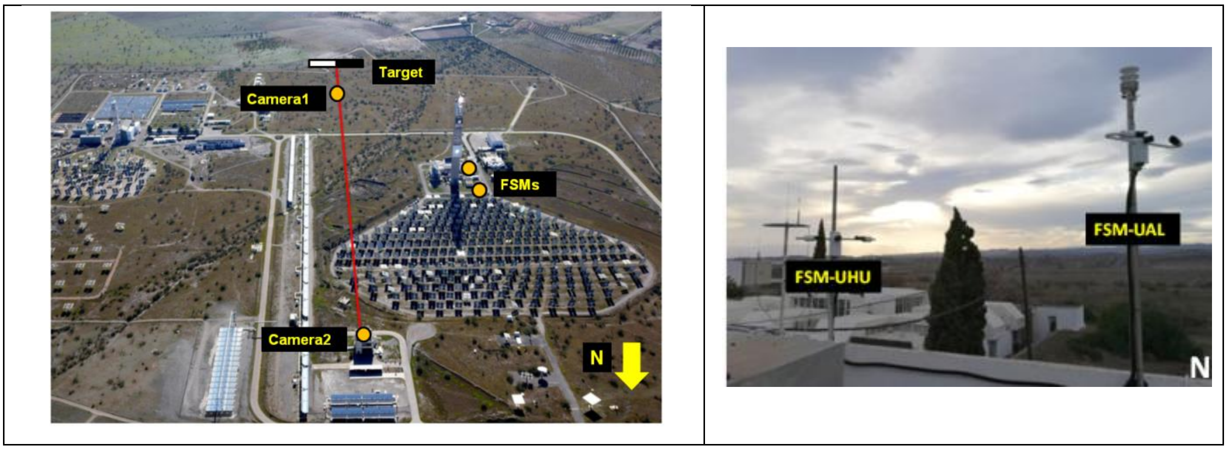

Figure 1. Left: layout of the CIEMAT-System and the two FSMs at PSA. Right: Biral SWS-250 FSMs belonging to the UAL and the UHU, placed at PSA facilities

To ensure the reliability of measurements, the calibration of both FSM was checked just before the beginning of the experimental campaign using the respective calibration plates provided by the manufacturer.

3.2 Data

The Biral SWS-250 provides MOR values in a range from 10 m to 75 km. The MOR measurement error ε_{MOR} is given by the manufacturer (O&M SWS Manual, 2014) up to MOR 30 km, but uncertainties for values above 30 km are unknown. Nevertheless, a first approximation of the uncertainties can be derived by linear extrapolation of documented uncertainty values in the whole range of 0-75 km, according to the following expression:

$$\varepsilon_{MOR}\ (\%) = 4.46 + 0.52\ \text{MOR (km)} \quad (2)$$

Throughout the test period, around 250 000 one-minute records corresponding to each one of the FSMs are available. Each MOR value is calculated as the average of 60 one-second values.

The CIEMAT-System takes data every minute between 10 to 15 h (local time), and supplies the value of the horizontal atmospheric attenuation (in %) for a distance of 742 m, along with its absolute error. During the test, 18 000 attenuation values were available from that system. A small amount of attenuation data was rejected due to undesirable situations, such as spurious radiation incidences on the target or reflections on the cameras coming from bright clouds.

During the period of time in which both systems were available, which covered about 160 days, there are simultaneous records of both systems in 91 days.

A collocated radiometric and meteorological station has also been used. It consists of a spectroradiometer EKO MS-700 (EKO, 2016) mounted on an EKO automatic solar tracker model STR-22G, and sensors for atmospheric variables (temperature, relative humidity, atmospheric pressure and wind speed and direction).

3.3 Data processing and selection

All data records were referred to the UTC time, and the days were referred to the first day of the year; thus, April 24th is day 114.

The data derived from the FSMs and the CIEMAT-System have been homogenized to represent the atmospheric attenuation of the solar radiation at 1 km distance, which is a representative distance in the tower plants. Therefore, the attenuation data of the CIEMAT-System, derived for a distance of 742 m, were converted to attenuation values at 1.0 km, through the extinction coefficient σ_{CSys}:

$$\sigma_{CSys}\ [\text{km}^{-1}] = -\ ln(1-Att(0.742))/0.742 \quad (3)$$

$$Att_{CSys}\ (1.0\ km) = 1-exp(-\sigma_{CSys}) \quad (4)$$

MOR values supplied by the FSMs were also converted to attenuation values at the distance of 1.0 km with the following expression:

$$Att_{FSM}\,(1.0\ km) = 1 - exp(ln(0.05)\ /\ MOR) \qquad (5)$$

Water vapour density at the surface, ρ_{w0}, has been used as an independent variable; although there is not a very significant difference with the relative humidity, *RH,* it is a variable proportional to the density of water vapour molecules. The following equations were used to calculate it (Gueymard, 1994):

$$\rho_{w0}\ [g\ cm^{-3}] = 216.7\ RH(\%)\ *\ p_s(hPa)\ /\ T(K) \qquad (6)$$

where T is the ambient temperature, and p_s is the saturation pressure, calculated as:

$$p_s\ [hPa] = 6.112\ exp(17.67*T(^{o}C)\ /\ (247.5 + T(^{o}C)) \qquad (7)$$

3.4. Intercomparison between forward-scatter meters

During the test campaign, FSMs frequently detected situations of very high visibility, displaying its limit value of MOR = 75 km. The equivalent atmospheric attenuation at 1 km then was less than 3.9%, as derived from Eq. (5). As the FSM only detects aerosol scattering at its sensitive volume, this is the minimum attenuation by aerosols at 1 km in the case of a homogeneous atmosphere equal to that surrounding the FSM. As a high variability was observed in the MOR measurements each minute, since they measure very local conditions, these measurements have been filtered by a 5 minute moving average filter.

The first step was to verify the consistency of the MOR data from both FSMs. Simultaneous data from both FSMs have been compared throughout the entire trial period. Figure 2 shows MOR records on April 24th and 25th, days included in an episode of dust intrusion. As it can be seen, a notorious decrease of visibility appeared in the morning of April 24th, reaching MOR values around 30 km. At the subsequent night, MOR values were as low as 2 km.

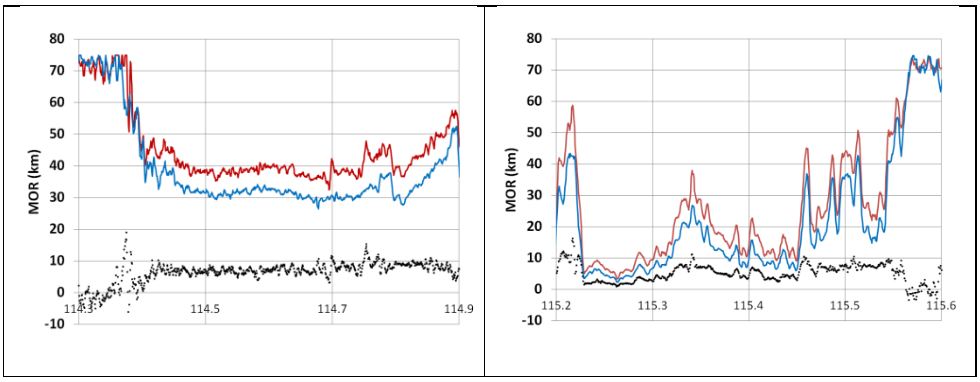

Figure 2. MOR values (km) for FSM-UAL (Red) and FSM-UHU (Blue) during April 24th (left) and April 25th (right), and difference between both FSMs (Black dots). Abscissa is day-of-year fraction (UTC).

Figure 2 shows the general behaviour of both FSMs observed throughout the trial, which is summarized in:

- The remarkable parallelism between both time series and the simultaneity of specific episodes.

- MOR values from FSM-UAL are systematically higher than the ones from FSM-UHU, up to 10 km for intermediate MOR values, but within the respective uncertainty limits.
- When both FSMs approach their detection limit of 75 km, there are no significant differences in measurements between them.

Due to the similar behaviour observed from both FSM, that the differences between their measurements are within the stipulated uncertainty ranges and the lack of additional criteria to decide which FSM has the best performance, a *virtual* FSM has been defined averaging the simultaneous MOR measurement from both FSMs.

3.5 Data selection

A set of days were selected to compare both systems. Only days that met the following conditions for most of the daytime were selected: CIEMAT-System attenuation values were taken in cloudless situations or with low presence of clouds, and FSMs' MOR values remained below 75 km most of the time. Only 11 days meet these requirements.

During the test campaign there have been some episodes with a medium to high aerosol load. Special attention was paid to these situations of high atmospheric extinction, as they represent the best opportunity to study the response of both systems. These episodes happened around April 20th, May 22nd and June 23rd. Another episode, although not as strong, happened from July 10th; in this case the CIEMAT-System registered attenuation values up to 13%. Only 8 days from the selected set of days that met the requirements are included in the cited episodes.

Figure 3 shows the Europe and North-Africa dust surface concentration (µg m^{-3}) maps provided by the AEMET-Barcelona Dust Forecast Center (BDFC, 2020) for the mentioned dust incursion episodes.

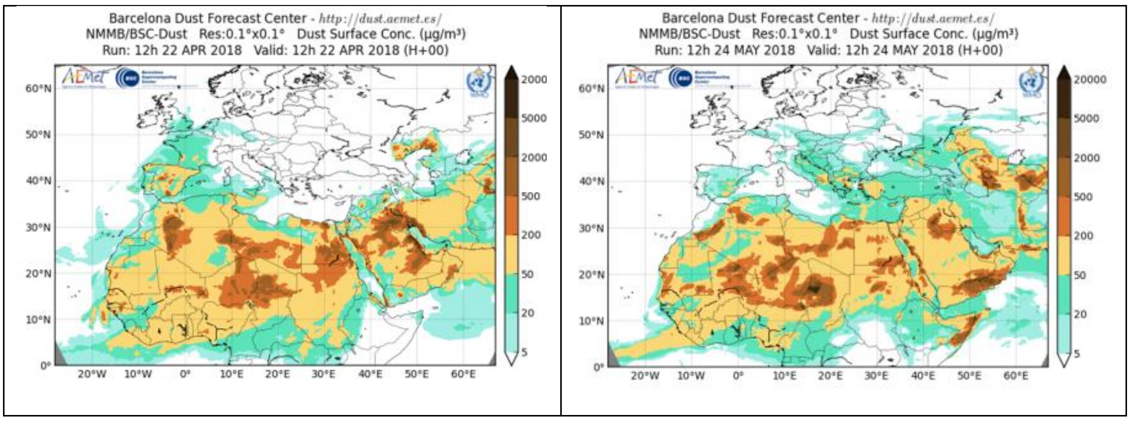

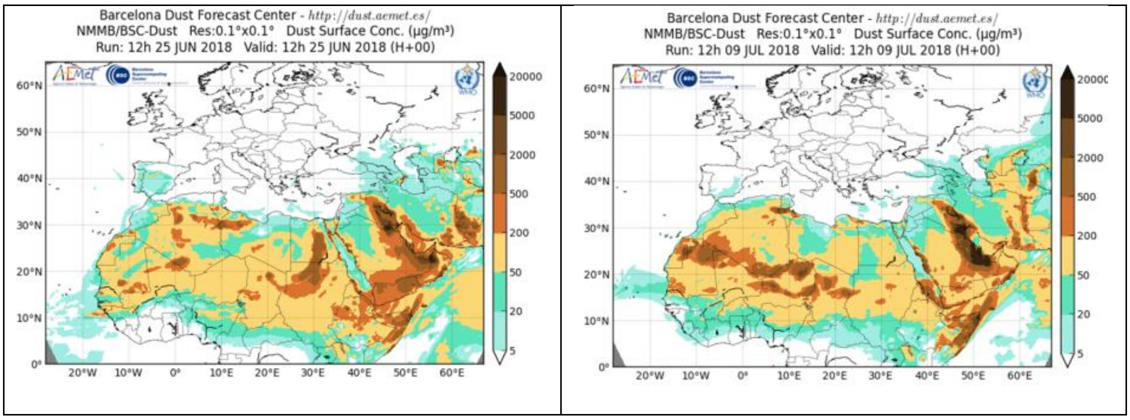

Figure 3. Dust surface concentration for days 22/4, 24/5, 25/6 and 9/7 of 2018. Source: AEMET-Barcelona Dust Forecast Center.

Table 1 summarizes the average values from the weather station and the collocated spectroradiometer for the 11 days that meet the requirements. Only 8 days included into the episodes were selected to develop the methodology and the other 3 days (in italic in Table 1) were used to check the derived algorithm.

Table 1. Average values from 10 to 13 h (local time) for air temperature, relative humidity, water vapour density at surface, aerosol optical depth at 500 nm and aerosol Ångström exponent. Data in parentheses is from AERONET_Murcia

Day	*T(ºC)*	*RH (%)*	$\rho_{w,0}$ *(g cm^{-3})*	AOD_{500}	α
April 20	16.7	56.6	8.2	043	0.35
April 24	23.0	34.5	7.0	0.28	0.21
April 27	20.7	59.4	10.4	0.23	0.81
May 18	20.4	47.6	8.3	0.06	1.54
May 21	20.1	46.8	8.6	0.17	1.38
May 25	21.8	51.5	9.7	0.21	0.70
May 29	21.8	46.9	8.8	0.17	1.01
June 26	28.8	44.6	12.4	0.29	0.39
June 29	26.9	53.4	13.4	0.30	1.05
July 10	30.5	35.1	10.6	0.14	0.54
July 12	30.7	30.2	9.3	(0.21)	(1.3)

AOD_{500} and aerosol Ångström exponent (α) have been derived from the direct normal irradiance spectra registered by the spectroradiometer, using the "window method" (Martínez-Lozano et al., 1998) in situations when the sun was not covered by clouds. On July 12th, when the spectroradiometer and also the AERONET_Tabernas station were unavailable, AOD_{500} and aerosol exponent registered at AERONET_Murcia (~150 km away) were used as reference.

4. Results

This section will present the results of the intercomparison between the previously presented atmospheric extinction measurement systems, which will also include a discussion of the most important and determining facts.

4.1 Attenuation measurement systems intercomparison.

Since the CIEMAT-System records the total extinction between cameras by air molecules (Rayleigh scattering), aerosols (absorption and scattering) and water vapour, it has been considered, in this test, as a reference equivalent to a long-base transmissometer. The reliability of the attenuation values provided by the CIEMAT-System at PSA has been tested against yearly horizontal attenuation values derived from a typical aerosol year (TAY) using the AOD values at different wavelengths from the AERONET_Tabernas station at PSA. Results show similar statistical values (histograms, mean and extreme values) for the TAY analysis and for the CIEMAT-System (Carra et al., 2018).

In the case of real-time values, an independent method has been used. Said method allows determining the attenuation value with a single digital camera, using landscape images which include the black side of the target and the sky just above the target. Attenuation values obtained during a test campaign on several July 2018 days were similar for the CIEMAT-System and single camera systems, always within the margins of error of both methodologies (Barbero et al., 2020).

Figure 4 shows daytime evolution of attenuation values provided by the CIEMAT-System and attenuation from the averaged FSM for the 8 selected days. The time interval spans from 8:30 to 13:30 (UTC), a somewhat broader range than the daily working time period of the CIEMAT-System. The attenuation uncertainty for the CIEMAT-System device has been estimated to be lower than 2.0% (Ballestrín et al., 2018a). For the FSM, using the extrapolated relative uncertainty data (Eq. 2), an absolute uncertainty at 1 km of 2.3% has been derived for MOR values between 20 and 70 km.

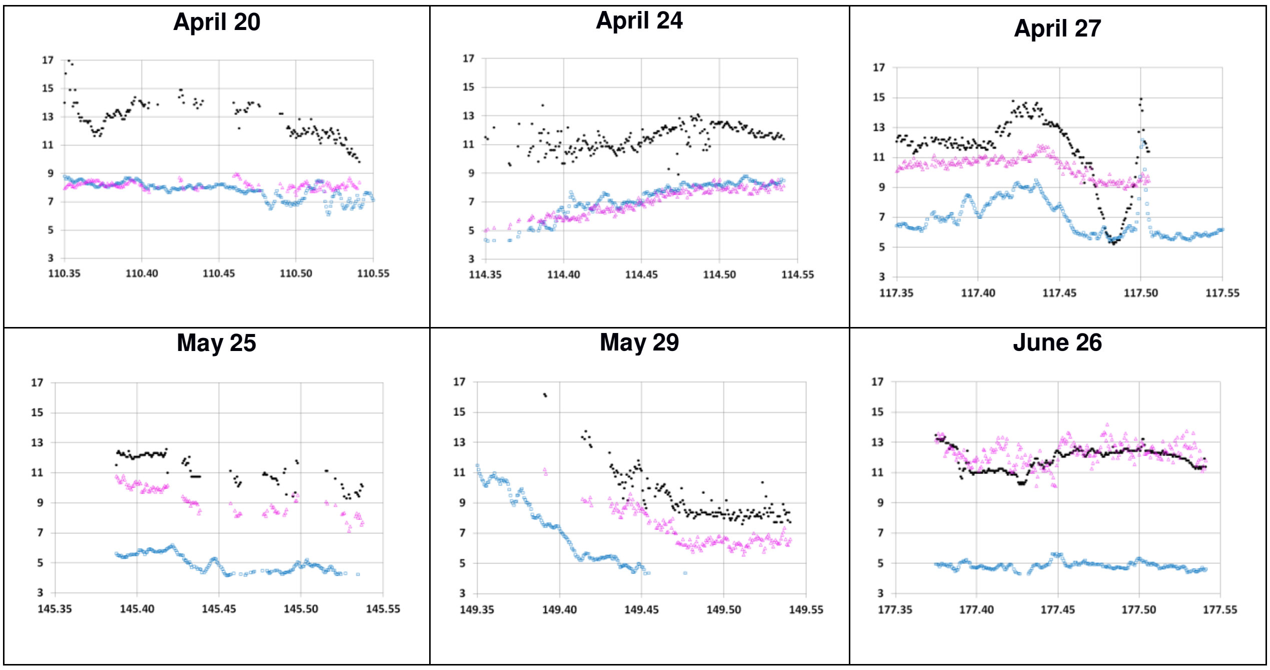

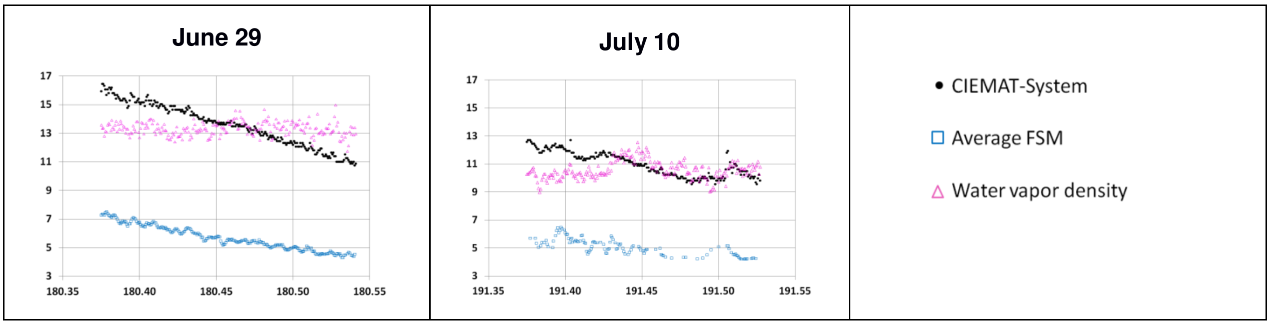

Figure 4. Attenuations (%) at 1 km: CIEMAT-System (black), average FSM (blue). Water vapour density at surface (g cm^{-3}) (purple) for the selected days. Abscissa in day-of-year fraction (UTC).

There is a lack of attenuation data in Figure 4 from the CIEMAT-System in some intervals; these data were rejected mainly due to saturation of images by high radiant flux from the target due to bright clouds behind the cameras. The existence of these clouds was confirmed by the discontinuous DNI records from pyrheliometers.

It is worth noting that the prevailing winds on the selected days have been from directions E and SW, induced by the topography of the valley in which the PSA is located. But no clear correlation has been found between fluctuations in wind speed and the visibility measured by the FSMs.

Several conclusions can be drawn from Figure 4 about the behaviour of both systems in the selected days:

- FSM attenuations at 1 km are always lower than the ones from the CIEMAT-System.
- When the CIEMAT-System gives attenuations below 9%, the FSM provides attenuation values of 3.9% that correspond to the MOR limit of 75 km.
- Attenuation values from the CIEMAT-System follow in most cases the long-time evolution of the water vapour density at the surface, and even some of the short-term water vapour variability (April 27th, May 29th).
- In the case of April 27th, just before 12:00 h, FSMs detected a brief episode of weak rain of about 10 minutes, although it was not registered by the PSA rain gauge. Consequences of this episode on the attenuation values were captured by both systems and CIEMAT-System and FSM systems provided very similar results.

4.2 Extinction coefficients ratio

Differences between the attenuation values at 1 km derived from the averaged FSM and the CIEMAT-System, shown in Figure 3, can be better expressed in terms of the ratio between their respective extinction coefficients. This ratio is written as follows:

$$\sigma_{CSys} / \sigma_{FSM} = ln(1-Att_{CSys}) / ln(1-Att_{FSM}) \quad (8)$$

where attenuations Att_x are defined in equations (4) and (5).

To evaluate the behavior of this relationship on each of the days, a time range has been selected from 10 to 13 h (local time). Using equation (8), the values of the ratio between both extinction coefficients were calculated for the time intervals in which there were measurements of both systems; then the average value of all of them was calculated. The results of this average, together with the standard deviation, are shown in Table 2.

Table 2. Average and standard deviation values of CIEMAT-System extinction coefficient ratio to the extinction coefficient from the averaged FSM, calculated from 10 to 13 h (local time).

Day	$\sigma_{CSys} / \sigma_{FSM}$	*StdDev*
April 20	1.81	0.07
April 24	1.73	0.19
April 27	1.64	0.11
May 25	2.32	0.14
May 29	2.29	0.14
June 26	2.58	0.11
June 29	2.52	0.07
July 10	2.25	0.05

An average value for all the selected days results in: $\sigma_{CSys} / \sigma_{FSM}$ = 2.1, with standard deviation of 0.4. Then the extinction coefficient values derived from the CIEMAT-System are, in average, around 2.1 times those derived from the FSMs. This remarkable discrepancy between the extinction coefficient values from both systems, also observed in Figure 4, deserves a detailed analysis.

The CIEMAT-System has a long baseline and wide spectral range, while the FSM samples over a small volume and it is almost monochromatic. FSM records only scattering by particles while the CIEMAT-System (or a broadband system working with a long baseline) can detect scattering and absorption by aerosols, molecular Rayleigh scattering and water vapour absorption. All these causes, related to the design and the operational characteristics of each one of the systems will be described in detail below. Figure 5 summarizes the process to be followed so that the Biral FSM monochromatic measurement may be validated against that broadband one provided by the CIEMAT-system.

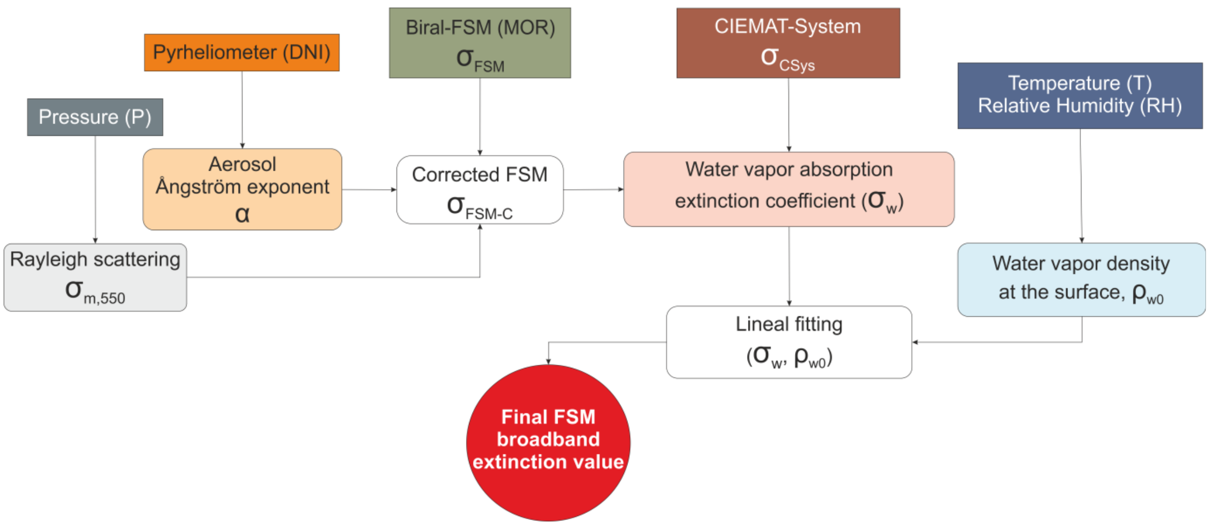

Figure 5. Flowchart showing the process to correct the FSM measurements. Both input extinction coefficients are referred to the distance of 1 km

The basic elements of this flow chart are developed in the following sections. An expression will be obtained that allows correcting the FSM measurements by parameters that come from the FSM design itself, and by other absorption and scattering phenomena detected by the CIEMAT System. Corrections to be made are: the Rayleigh scattering by air molecules (Section 4.3) and the dependence of the FSM measurement on the type of aerosol (Section 4.4). Once these corrections were made, a further correlation of σ_{CSys} - $\sigma_{FSM\text{-}c}$ with the water vapour density at the surface will be found (Section 4.5). Using this correlation, the FSM measurement can also be corrected for water vapour absorption.

4.3 Rayleigh scattering by air molecules

Given the small sensitive volume of the FSM, it does not register the Rayleigh scattering by air molecules, whereas the CIEMAT-System does due to its much greater operating distance. Then, the extinction coefficient derived from the FSM must be corrected with the Rayleigh scattering extinction coefficient modified according to the actual atmospheric pressure value.

A standard value of $\sigma_{m,550}$ = 0.01149 km^{-1} was taken from literature (Bucholtz, 1995), and then corrected by the measured value of the atmospheric pressure at site. At PSA site, 500 m a.s.l., with average pressure of 967 mbar, attenuation values at 1 km due to Rayleigh scattering were 1.1%. At sea level this attenuation at 1 km is an offset of 1.2%.

4.4 FSMs data correction under haze conditions

In this section the corrections in the measures when haze conditions are present in the atmosphere are analyzed.

4.4.1 Correction factors from FSM M&O manual

A important cause to explain these discrepancies may come from the own design of the FSM. Primarily designed to provide visibility values in fog or mist conditions, FSMs would not provide adequate MOR values in haze situations. The scattering angles selected in the FSM design are between 30º and 50º. At these angles, an FSM provides scattering values that are almost independent of particle size, but the value of the scattering function that is used to convert the FSM output to the integrated scattering at all angles is that for fog, which has a lower value than that for fog.

In the basic manual of its operation, the manufacturer refers to some corrections that must be made to have adequate values in cases of haze when an FSM Biral has been calibrated in fog conditions. In case of a haze situation, the value of the extinction coefficient provided by the FSM must be multiplied by the relation between the dispersion phase function at 45º for the haze with that corresponding to fog. This haze-to-fog conversion factor (*StF*) is 0.58 in case of FSM Biral (Biral Present Weather Sensors, 2017).

Additionally, because of the aerosol scattering coefficient depends on wavelength, a further correction factor must be applied to change from the infrared spectral range where the SWS-250 registers scattering (850 nm) to visible range (550 nm) as follows:

$$F_{\lambda} = (550/850)^{-\alpha} \qquad (9)$$

where α is the aerosol Ångström exponent.

It is worth to note that the spectral range correction factor almost exactly compensates the haze-to-fog conversion factor in the case of atmospheric aerosols with Ångström exponent 1.3 (F_λ = 1.76). This is equivalent to saying that in case of small aerosol particles, according to its M&O manual, this FSM should provide direct aerosol attenuation values. But in the general case, the correction to the FSM measurement shall depend on the type of aerosols present.

4.4.2 Correction factors derived from the FSM modelisation

In another line of research (Elias et al., 2017), the response of three different FSM models to different types of aerosols (dry mist, hydrated aerosols, mist and desert dust) has been modeled using Mie's theory. These three FSM were: Biral-VPF710 at 875 nm (Biral Present Weather Sensor, 2017), Vaisala-FS11 (Vaisala, 2010), at 850 nm and Degreane-DF20+ at 550 nm (Degreane, 2007). They obtained correction parameters for the measurements of each one of the referred FSMs, with special emphasis on the FSM Biral-VPF710, which is very similar to Biral-SWS250

Some results are in agreement with the referred Biral M&O manual, e.g. that the corrections to be applied in case of haze depend on the type of aerosol present. But they also conclude with some differences: 1) a correction factor should be applied to take into account the aerosol absorption (which can be calculated from the aerosol single scattering albedo, SSA); 2) the parameter to correct the FSM measurements from fog to haze seems to be also depends on the aerosol type.

4.4.3 Correction Algorithm to FSM MOR data, including Rayleigh scattering

Considering both the dependences on aerosol type and Rayleigh scattering, a whole correction of the FSM extinction coefficient can be performed with the following algorithm:

$$\sigma_{FSM\text{-}c}[\mathrm{km}^{-1}] = ln(0.05)/MOR * StF * F_\lambda * Acf + \sigma_{m,550} \quad (10)$$

$$Ktot = StF * F_\lambda * Acf \quad (11)$$

The corresponding aerosol Ångström exponent value for the aerosol column in Table 1 has been used to compute the wavelength dependent correction factor defined in equation (9), F_λ.

The first term of the sum on the right side of equation (10), corresponds to the correction on the FSM measurement changing to the visible range and including aerosol absorption. The aerosol absorption correction factor has been taken as 1.06, corresponding to a SSA = 0.94, which is an adequate value for the typical aerosols at PSA (rural, tropospheric and maritime) and also for STEP emplacements (Shettle & Fenn. 1979).

Table 3 shows the values of *StF*, F_λ, *Acf* and *Ktot* parameters for the Biral FSM for different aerosol exponent values corresponding to standard (fine) aerosols (*BMod-fine*); α = 0.0 aerosols (*BMod-coarse*) and any exponent (*BMod*), and also using the model *EMod* (Elias et al., 2017).

Table 3. Correction factor *Ktot* for the Biral FSM values for different aerosol models.

	Haze

	StF	F_λ	Acf	Ktot
BMod-fine, α = 1.3	0.58	1.76	1.06	1.08
BMod-coarse, α = 0.0	0.58	1.00	1.06	0.62
Bmod	0.58	F_λ	1.06	0.62 F_λ
EMod	0.49	2.8	1.06	1.45

As it can be seen, the *Ktot* value for the *Bmod-fine* case (1.08) leaves the FSM measurements almost unchanged, and in case of coarse aerosols the correction gives even lower attenuation values than the measured ones prior to the addition of the Rayleigh scattering extinction coefficient $\sigma_{m,550}$.

4.5 Water vapour density at surface dependence

The FSM measurements have been corrected for each day using the algorithm of equation (10) in three situations; applying *EMod*, *BMod-fine* and *BMod*, the latter being the one that uses the Ångström exponent values in Table 1.

Scattering and absorption by aerosols and also scattering by air molecules have already been considered in the corrected FSM values at equation (10). The discrepancies that continue to be observed between the CIEMAT-System and corrected FSM extinction coefficients could be explained by the contribution of the water vapour absorption at the surface, which is detected by the CIEMAT-System but not by the FSM.

The relationship between the horizontal attenuation of the reflected radiation by the heliostats and the water vapour content in case of an aerosol free atmosphere has been modeled using a radiative transfer code (López et al., 2018a). The water content ranges from a extreme dry atmosphere (w = 0 cm) to a subtropical atmosphere (w = 4.5 cm). One of the main results is that the horizontal attenuation is not linearly correlated with the water vapour content; transmission losses for high w values only slightly increase respective to medium w values. The explanation is that for high w values the incident solar spectrum on the heliostat has already been severely attenuated by the atmosphere in the water vapour absorption bands; therefore the water vapour between heliostat and receiver scarcely contributes to the attenuation in high water vapour content situations. In that study, an attenuation value of 3.5% was calculated at 1 km for an aerosol free atmosphere with w = 1.42 cm, equivalent to a water vapour density at surface of 6.8 g cm^{-3} for water vapour scale height of 2.1 km (Gueymard, 1994). As the Rayleigh scattering attenuation at 1 km was around 1%, the contribution of water vapour must account for the remaining 2.5%.

Although the relationship between both variables is not linear, we consider that for the water vapour content values in the selected days, between 1.3 and 3.5 cm, it is possible to find a linear relationship between the water vapour extinction coefficient and the water vapour density at surface in the form:

$$\sigma_w = \sigma_{CSys} - \sigma_{FSM\text{-}c} = a\,\rho_{w0} + b \qquad (12)$$

The relationship has been calculated for the selected days, resulting in 862 pairs of data for each model. Table 4 shows the results for the linear correlation coefficients.

Table 4. Linear fitting parameters for different models to derive the water vapour absorption coefficient at PSA

	a (10^{-3})	b (10^{-2})
EMod	7.48	- 4.98
BMod	3.81	2.74
BMod-fine	6.68	- 2.08

When compared with the previous cited value of 3.5% López et al. (2018a), it was found that the *BMod* model gave the most similar approach to the water vapour contribution.

Then, the algorithm which would translate the FSM MOR measurement to a broadband extinction coefficient, $\sigma_{FSM,BB}$, taking into account all corrections, may be written as:

$$\sigma_{FSM,BB}\,[\mathrm{km}^{-1}] = ln(0.05)/MOR * StF * F_{\lambda} * Acf + \sigma_{m,550} + (a\,\rho_{w0} + b) \quad (13)$$

Figure 6 shows the comparison between the CIEMAT-System attenuation at 1 km and those derived from the full corrected FSM measurement for *EMod* and *BMod* models, including the corresponding to water vapour density at surface values obtained from parameters in Table 4.

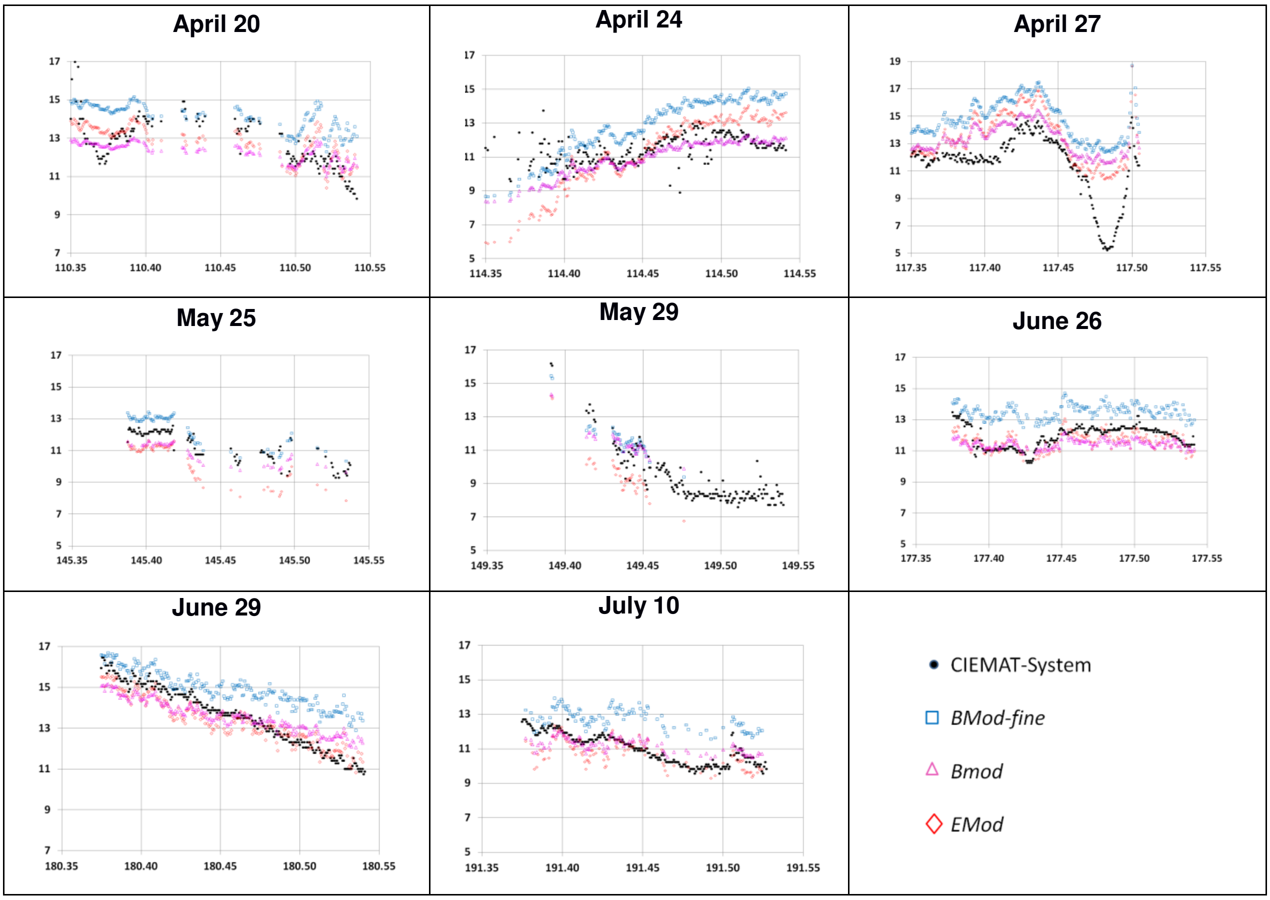

Figure 6. Horizontal attenuations at 1 km (%): CIEMAT-System (Black) and FSM corrected models *EMod*, *BMod* and *BMod-fine*. Note that the ordinate scale is not as in Figure 4, but expanded to better see the differences among models.

To test the goodness of the different models, an independent set of days not used to carry out the process described above, has been utilized. These days are May 18th, May 21st and July 12nd. Averaged daytime values for meteorological relevant variables can be found in Table 1. It is worth noting that in these days the Ångström exponent correspond to fine aerosols.

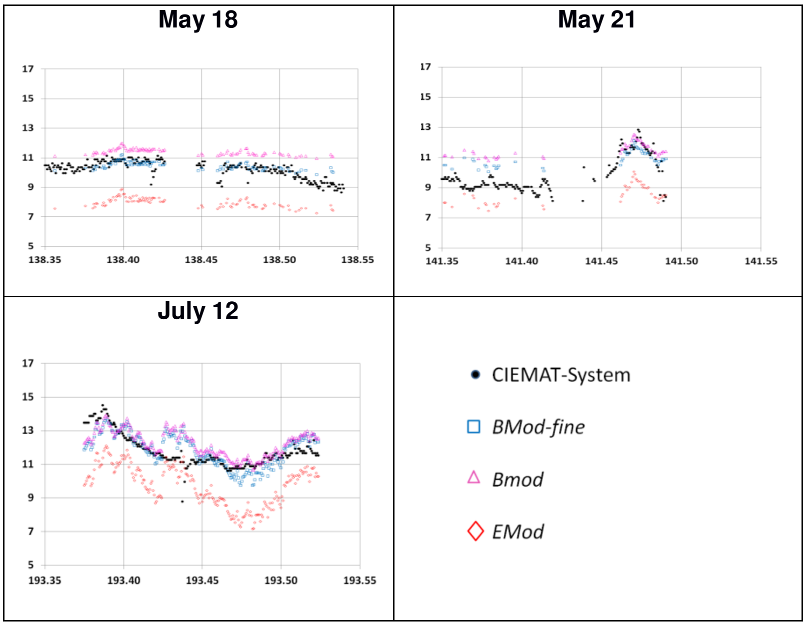

Figure 7. Horizontal attenuations at 1 km (%): CIEMAT-System (Black) and FSM corrected models *EMod*, *BMod* and *BMod-fine* for validation days

Table 5 resumes the total extinction coefficient ratio CIEMAT-System to each one the corresponding to the models for all the selected days. "Set 1" is for the eight days in Figure 4 and "Set 2" is for the three test days.

Table 5. Average and standard deviation values from 10 to 13 h (local time) of CIEMAT-System extinction coefficient ratio to the extinction coefficient from each one of models for all the selected days.

Set	$\sigma_{CSys} / \sigma_{BModfine}$	$\sigma_{CSys} / \sigma_{BMod}$	$\sigma_{CSys} / \sigma_{EMod}$
Set 1	0.92 (0.03)	1.06 (0.04)	1.10 (0.06)
Set 2	0.99 (0.06)	0.92 (0.06)	1.18 (0.03)

Figure 6 and data in Table 5 show how the *BMod* model, that considers the correction due to the derived aerosol Ångström exponent at the atmospheric column and from the corresponding coefficients in Table 4, seems to be the best one (averaged extinction coefficients ratio 1.06) to approach the CIEMAT-System attenuation measurements for the Set 1 days. But, the *EMod* may also give reasonable results. The *BMod-fine* seems to be the worst performing in these dusty days, with low aerosol Ångström exponent values.

In case of Figure 7 and data in Table 5, it is shown how the fit with *BMod* and also with *BMod-fine* are good for the determination of the horizontal attenuation. The similarity of behaviour of both models is not surprising because the Set 2 days were days in which the aerosols showed a Ångström exponent of the order of 1.0, while the *BMod-fine* model was for aerosol exponent 1.3. Results with *EMod* underestimate the extinction coefficient around 20 %.

We are considering only horizontal extinction measurements at the surface but, at this point, it is important to evaluate also the contribution of the vertical extinction, because in a STP of 100 MW, the central receiver is located as high as 250 m above the surface or even more. To estimate the influence of the receiver height on the total extinction some published results (Ballestrín et al, 2016) can be used. DNI spectral radiative transfer calculations with MODTRAN code (Anderson et al, 1996) at the base of the tower and at 100 m above have been carried out for three different visibilities (VR = 5 km, 23 km and 50 km) and for a homogeneous rural atmosphere. Results show that attenuation values of solar spectra were 3.5%, 0.6%, 0.25%, respectively. It can be estimated that, in the case of VR = 23 km (MOR = 17 km) and a receiver height of 200 m, there would be a vertical attenuation of 1.5%. For a STEP with heliostats 1 km away, and under the same conditions, these would suffer much higher horizontal attenuation levels, so the vertical contribution would be negligible. This vertical component could be relevant in the case of the closest heliostats, generally at horizontal distances equivalent to the height of the tower, but their number is small, so their influence on the final contribution to the energy produced would be very low.

It is usual to work with the hypothesis of atmosphere homogeneity of the lowest aerosol layer up to heights above the receiver. However, knowing the height profile of the aerosols could be important in the referred case of a receiver 200 m above the level of the heliostats. Using a Vaisala CL51 (Vaisala CL51, 2010) ceilometer, concentration fluctuations with root-mean-square error up to 10% around 1-hour moving average have been observed at 100 m above ground in case of high dust density near the surface (Barbero et al, 2018). This ceilometer is characterized by having a full overlap height around 80 m. The use of a collocated lidar with this feature could report in near real time the profile of the aerosols from full overlap height to well above the receiver.

5. Conclusions and outlook

Determination of the attenuation of solar radiation between the heliostats and receiver in a STP is important to evaluate the efficiency of the heliostat field and, therefore, the efficiency of the plant itself. Quality measurements are necessary to quantify the attenuation in real time but also to generate and validate models that allow estimation of attenuation from other parameters. In this context, an intercomparison campaign has been carried out between two methodologies for determining the extinction of solar radiation in the lower layers of the atmosphere.

One of the methodologies, developed at PSA-CIEMAT, consists of a set of two cameras (CIEMAT-System), spaced at a distance of 742 m, which simultaneously acquires the image of a Lambertian target, painted in white and black. This methodology directly provides values of horizontal atmospheric attenuation using a baseline close to 1 km.

The other methodology is based on FSMs, monochromatic instrumentation that are commonly used to measure visibility conditions in airports and highways. Two identical FSMs and the CIEMAT-System PSA-CIEMAT system were used in the intercomparison.

In the case of the two FSM it was observed that they fitted to each other within the respective uncertainty margins. However, the extinction coefficients obtained from their MOR values were on average a factor 2.1 lower than those provided by the CIEMAT-System. This discrepancy can be explained because an FSM measures particle scattering in a small volume and it is designed to provide the most reliable output in low visibility fog and mist situations but it overestimates visibility in haze conditions. From the underlying physical phenomena, the discrepancy occurs because an FSM records only scattering, while the CIEMAT-System (or a broadband system in general) can detect scattering and absorption by aerosols, Rayleigh scattering by air molecules and water vapour absorption. The process to correct the measurement of an FSM for all these effects has been summarized in the flowchart in Figure 5.

To correct the values of σ_{FSM}, several correction factors must be applied: some are documented for each FSM model, and others depending on the emplacement. Although general guidelines can be given:

The haze-to-fog correction factor, *StF*, depends on the angle between the emitter and the receiver of the FSM. In general, this design angle is between 30º and 50º, because in this range of angles the scattering coefficient has a very low dependence on the size of the aerosols. See as an example in Table 3 the calculated values of this factor for two different infrared FSMs.

The wavelength correction factor F_λ depends on the Angstrom exponent of the aerosols (equation 9) however, since IR FSMs all work at very similar wavelengths, this factor will be almost identical for all of them.

The corrective term for aerosol absorption, *Acf*, for sites with rural, tropospheric or maritime aerosols, and with relative humidity around 50%, this value is between 1.0 and 1.06. However, for urban type aerosols this value increases to 1.54 (Settle & Fenn, 1979).

The correction for the Rayleigh scattering of air molecules depends on the atmospheric pressure at the site, but can be considered as an offset. At sea level, represents an attenuation of 1.2% at 1 km

Finally, absorption by surface water vapour is conditioned by the characteristics of the site, and is calculated according to equation 12. In the case of PSA, in these episodes has been between 5.5 and 14.7 g cm^{-3}; these values correspond to a precipitable water amount in the atmosphere between 1.3 and 3.5 cm, for a water vapour scale height of 2.4 km.

In the analyzed cases, the best solution for estimating real-time attenuation values from Biral FSM measurements should be to correct these values using equation (13) with the model *BMod* parameters, when the aerosol Ångström exponent is known (from a collocated spectroradiometer or a near AERONET station), and the corresponding correction by water vapour density at surface obtained from Table 5. But horizontal attenuation at 1 km forecasting with 2% of absolute error could be also achieved using *BMod* with $\alpha = 1.0$.

FSMs allow estimating the aerosol concentration in the local atmosphere, but its use to get reliable horizontal attenuation values (even with considerable error margins) is very complex. The corrections to be applied to the visibility provided by that equipment are based on empirical or semi-empirical models, which need to know the nature of the aerosol present. This information is not commonly known at the location of a solar plant and, in the best case, is obtained from the direct normal solar radiation through the atmospheric air column, and not from surface-level aerosol data.

The best solution is to have instrumentation that directly provides broadband horizontal attenuation, such as the CIEMAT-System. But it is possible to maximize the utility of a FSM to determine real-time values at a solar central tower plant including its MOR measurement in an artificial neural network structure, along with other meteorological and radiometric variables (direct solar radiation, relative humidity, temperature and pressure).

Acknowledgements

This work is included in the activities of the PRESOL project (Forecast of Solar Radiation at the Receiver of a Solar Power Plant) funded by the Spanish Government (Ref. ENE2014-59454-C3-1, 2, 3-R). And also the PVCastSOIL Project (Ref. ENE2017-83790-C3-1, 2, 3), funded by the Spanish Government and co-financed by the European Regional Development Fund.

The authors acknowledge the financial support provided by the Innova Chile - CORFO, PROJECT CODE: 17BPE3-83761, as well as CONICYT/FONDAP/15110019 “Solar Energy Research Center” SERC-Chile.

The authors wish to thank to the investigators involved in the stations at AERONET_Tabernas and AERONET_Murcia, for delivering so useful data.

And also wish to thank the PSA's Maintenance and Instrumentation staff for the excellent work during the preparation of the intercomparison tests.

References

Alonso-Montesinos, J, Ballestrín, J, López, G, Carra, E, Polo, J, Marzo, A, Barbero, J., Batlles, F.J.. 2021. The use of ANN and conventional solar-plant meteorological variables to estimate atmospheric horizontal extinction. Journal of Cleaner Production 285, 125395

Anderson, G.P., et al., 1996. Reviewing atmospheric radiative transfer modeling: new developments in high and moderate resolution FASCODE/FASE and MODTRAN. Proc SPIE 2830, Optical Spectroscopic Techniques and Instrumentation for Atmospheric and Space Research II, 1996; https://doi.org/10.1117/12.256105

Ballestrín, J. Marzo, A. 2012. Solar radiation attenuation in solar tower plants, Sol. Energy 86, 388-392.

Ballestrín, J., Monterreal, R., Carra, M.E., Fernandez-Reche, J., Barbero, J., Marzo, A. 2016. Measurement of Solar Extinction in Tower Plants with Digital Cameras. AIP Conference Proceedings 1734, 130002; doi: 10.1063/1.4949212

Ballestrín, J., Monterreal, R., Carra, M.E., Fernandez-Reche, J., Polo, J., Enrique, R., Rodríguez, J., Casanova, M., Barbero, F.J., Alonso-Montesinos, J., López, G., Bosch, J.L., Batlles, F.J., Marzo, A. 2018. Solar extinction measurement system based on digital cameras. Application to solar tower plants. Renew. Energy 125, 648-654. ISSN: 0960-1481, https://doi.org/10.1016/j.renene.2018.03.004.

Ballestrín, J., Carra, E., Enrique, R., Monterreal, R., Fernández-Reche, J., Polo, J., Casanova, M., Barbero, F.J., Marzo, A. 2018. Diagnosis of a Lambertian target in solar context, Measurement 119, 265-269. ISSN: 0263-2241, https://doi.org/10.1016/j.measurement.2018.01.046.

Ballestrín, J., Carra, E., Monterreal, R., Enrique, R., Polo, J., Fernández-Reche, J., Barbero, F.J., Marzo, A., Alonso-Montesinos, J., López, G., F.J. Batlles, F.J. 2019. One year of solar extinction measurements at Plataforma Solar de Almería. Application to solar tower plants. Renew Energy 136, 1002-1011

Ballestrín, J., Carra, E., Alonso-Montesinos, J., López, G., Polo, J., Marzo, A., Fernández-Reche, J., Barbero, F.J., Batlles, F.J. 2020. Modeling solar extinction using artificial neural networks. Application to solar tower plants. Energy. DOI: https://doi.org/10.1016/j.energy.2020.117432

Barbero, J., Alonso-Montesinos, J., Batlles, F. J., Polo, J., López, G., Bosch, J. L., Ballestrín, J., Carra, M. E., Fernández-Reche, J. 2018. Evolution of the aerosol extinction coefficient at 100 m above ground during an episode of Saharan dust intrusion as derived from data registered by a ceilometer in Almería (SE Spain). AIP Conference Proceedings 2033, 190002; https://doi.org/10.1063/1.5067187

Barbero, F.J., Alonso-Montesinos, J., Ballestrín, J., Carra, E., Fernández-Reche, J. 2020.Atmospheric horizontal extinction determined with a single digital camera-based system in the scope of solar power tower plants. Measurement 149, 107025, ISSN: 0263-2241 https://doi.org/10.1016/j.measurement.2019.107025.

Barcelona Dust Forecasting Center. https://dust.aemet.es/. Access 2021.

Biral VPF Series. Present Weather Sensors. Manual Number: 102186. 2017.

Bloemink, H.I. 2006. KNMI visibility standard for calibration of scattermeters. https://www.wmo.int/pages/prog/www/IMOP/publications/IOM-94-TECO2006/P3(26)_BloeminkMs_Netherlands.pdf

Bucholtz, A. 1995. Rayleigh-scattering calculations for the terrestrial atmosphere. Applied Optics, 34 n15, 2765.

Carra, E., Ballestrín, J., Polo, J. Barbero, F.J. Fernández-Reche, J. 2018. Atmospheric extinction levels of solar radiation at Plataforma Solar de Almería. Application to solar thermal electric plants. Energy 145, 400-407.

Chen, X., Lu, C., Liu, W., Zhang, Y. 2013. A New Algorithm for Calculating the Daytime Visibility Based on the Color Digital Camera. IJCSI International Journal of Computer Science Issues, Vol. 10, Issue 1, No 1. ISSN (Print): 1694-0784 | ISSN (Online): 1694-0814.

Degreane Horizon. User's Manual DF20+. 2007

EKO. MS-700 Spectroradiometer.pdf. https://eko-eu.com. 2016.

Elias, T., Ramon, D., Dubus, L., Brau, J., Langouet, H. 2017. Instrumental Set-up to Estimate the Atmospheric Attenuation along the Slant Path of Concentrated Solar Plants. In Proceedings of the Poster, SolarPACES2017, Santiago de Chile, Chile, 26–29 September 2017.

Gueymard, C. 1994. Analysis of monthly average atmospheric precipitable water and turbidity in Canada and Northern United States. Sol. Energy 53, 57-71.

Guide to Meteorological Instruments and Methods of Observation. World Meteorological Organization, 2014. 291-309.

Hanrieder, N., Wilbert, S., Mancera Guevara, D., Buck, R., Giuliano, S., Pitz-Paal, R. 2017. Atmospheric extinction in solar tower plants-A review. Sol. Energy 152, 193–207.

Hanrieder, N., Wehringer, F., Wilbert, S., Wolferstetter, F., Pitz-Paal, R., Campos, A., Quaschning, V. 2012. Determination of beam attenuation in tower plants. In: SolarPACES. Marrakech, Morocco

Hanrieder, N., Wilbert, S., Pitz-Paal, R., Emde, C., Gasteiger, J., Mayer, B., Polo, J. 2015. Atmospheric extinction in solar tower plants: absorption and broadband correction for MOR measurements. Atmos. Meas. Tech. vol. 8, no. 8, 3467–3480.

Hanrieder, N., Ghennioui, A., Merrouni, A., Wilbert, S., Wiesinger, F., Sengupta, M., Zarzalejo, L., Schade, A. 2019. Atmospheric Transmittance Model Validation for CSP Tower Plants. Remote Sens. 11 (2019)1083

Koschmieder, H. 1924.Theorie der horizontalen Sichtweite. Beitraege zur Physik der freien Atmosphäre, 12, 33–53.

López, G., Bosch, J.L., Pulido-Calvo, I., Gueymard, C.A. 2017a. Visibility estimates from atmospheric and radiometric variables using artificial neural networks. WIT Transactions on Ecology and The Environment, Vol 211, www.witpress.com, ISSN 1746-448X (on-line). doi:10.2495/AIR170131

López, G., Gueymard, C.A., Bosch, J.L. 2017. Evaluation of Solar Energy Losses for the Heliostat-to-Receiver Path of a Tower Solar Plant for Different Aerosol Models. SWC 2017 / SHC 2017 / ISES Conference Proceedings. doi:10.18086/swc.2017b.23.03.

López, G., Gueymard, C.A., Bosch, J.L., Rapp-Arrarás, I., Alonso-Montesinos, J., Pulido-Calvo,I., Ballestrín, J., Polo, J., Barbero, F.J., 2018a. Modeling water vapour impacts on the solar irradiance reaching the receiver of a solar tower plant by means of artificial neural networks. Sol. Energy 169, 34–39

López, G., Christian A. Gueymard, Juan L. Bosch, Joaquín Alonso-Montesinos, Igor Rapp-Arrarás, Jesús Polo, Jesús Ballestrín, Javier Barbero, Manuel J. Caro-Parrado, Francisco J. Batlles. 2018b. Estimation of Visibility from Spectral Irradiance Using Artificial Neural Networks. AIP Conference Proceedings 2033, 040023; https://doi.org/10.1063/1.5067059. Published Online: 08 November 2018.

Martínez-Lozano, J.A., Utrillas, M.P., Tena, F., Cachorro, V.E. 1998. The parameterisation of the atmospheric aerosol optical depth using the Ångström power law. Solar Energy. Volume 63, Issue 5, November 1998, Pages 303-311

Marzo, A., Salmon, A., Polo, J., Ballestrín, J., Soto, G., Quiñones, G., Alonso-Montesinos, J., Carra, E., Ibarra, M., Cardemil, J., Fuentealba, E., Escobar, R. 2021. Solar extinction map in Chile for applications in solar power tower plants, comparison with other places from sunbelt and impact on LCOE. Renewable Energy 170, 197-211 ISSN 0960-1481. Doi: https://doi.org/10.1016/j.renene.2021.01.126.

Middleton, W.E.K. 1952. Vision through Atmosphere. University of Toronto Press.

Pitman, C.L., Vant-Hull, L.L. 1982. Atmospheric transmittance model for a solar beam propagating between a heliostat and a receiver. ASES Progress in Solar Energy 1247-1251.

Operations and Maintenance Manual: SWS Present Weather Sensors. 2014. Bristol Industrial and Research Associates Limited (BIRAL).

OPTEC. 2011. Model LPV3 and Model LPV4. Long Path Visibility Transmissometer, Technical Manual for Theory and Operation and Operating Procedures, Technical report, 1-72.

Plataforma Solar de Almería. Annual Report 2018. http://www.psa.es/en/techrep.

Shettle, E., Fenn, R.1979. Models of the atmospheric aerosols and their optical properties. Environ. Res. 94.

Tjugum, S.A., Vaagen, J.S., Jakobsen, T., Hamre, B.. 2005. Use of optical scatter sensors for measurement of visibility. J. Environ. Monit. 7, 608-611

Vaisala. 2010. User's Guide: Present Weather Sensor FS11P.

Vaisala ceilometer CL51. User's guide. Functional description. 2010.

Wang, J., Liu, X., X. Yang, X., M. Lei, M., Ruan, S., Nie, K.,Miao, Y., Liu, J. 2014. Development and evaluation of a new digital photography visiometer system for automated visibility observation. Atmospheric Environment. 87, 19-25. https://doi.org/10.1016/j.atmosenv.2013.12.045